Available online at www.sciencedirect.com
SCIENCE DIRECT®
International Journal of Heat and Mass Transfer 47 (2004) 5565–5574
International Journal of HEAT and MASS TRANSFER
www.elsevier.com/locate/ijhmt

Effective thermal conductivity of wet particle assemblies

M. Kohout [a], A.P. Collier [b], F. Štěpánek [a,*]

[a] Department of Chemical Engineering, Imperial College London, South Kensington Campus, London SW7 2AZ, United Kingdom
[b] GlaxoSmithKline R&D Ltd., Temple Hill, Dartford, Kent DA1 5AH, United Kingdom

Received 22 October 2003
Available online 16 September 2004

Abstract

The effective thermal conductivity of mono- and poly-dispersed random assemblies of spherical particles and irregular crystals, both dry and partially or fully saturated by wetting and non-wetting liquids, has been determined computationally by numerical solution of the Fourier's law on 3-D reconstructed media and experimentally by the transient hot wire method. The effect of spatial distribution and volume fractions of the vapour, liquid, and solid phases on effective thermal conductivity was systematically investigated. A power-law correlation for estimating the effective conductivity, valid over a wide range of phase volume fractions and relative conductivities of components, has been proposed.

Keywords: Contact drying; Thermal conductivity; Particle packing; Reconstructed porous media; Computer simulation; Hot wire method

1. Introduction

This work was motivated by the need to describe the unit operation of contact drying, which is often used for the removal of residual solvent from filter cakes during the manufacture of various crystalline chemicals such as active pharmaceutical ingredients. The heat necessary for the evaporation of the solvent is supplied to the wet particle mass via a heat-exchange surface, typically a vessel jacket. In the initial "constant-rate" period of drying, the drying process is limited by heat transfer; the overall heat-transfer coefficient depends on the effective thermal conductivity [1].

The effective thermal conductivity of a wet mass of particles depends on the thermal conductivities of its components (the gas, liquid, and solid phase), on their phase volume fractions, and on the microstructure (i.e. the spatial distribution of all the three phases). The microstructure of a wet particle assembly can be relatively complex [2,3]. A schematic microstructure is shown in Fig. 1 and several examples of microstructures used in this work for the calculation of effective thermal conductivity are shown in Fig. 4. The particle size and shape distributions mainly determine the packing density and the mean particle coordination number, while the spatial distribution of the liquid phase within the particle assembly depends on the liquid–gas interfacial tension and the equilibrium contact angle, as well as on the particle morphology.

As drying proceeds, all these parameters can—and often do—change as a result of particle agglomeration or breakage, solvent evaporation and subsequent solid re-crystallisation, etc. If one wishes to describe the drying process accurately, it is desirable to have a means

* Corresponding author. Tel.: +44 20 7594 5608; fax: +44 20 7594 5604.
E-mail address: f.stepanek@imperial.ac.uk (F. Štěpánek).

0017-9310/$ - see front matter
doi:10.1016/j.ijheatmasstransfer.2004.07.031

Nomenclature

A	unit cell size cross-sectional area, m^2
c	exponent in power-law correlation
L	unit cell size, m
$\dot{Q}$	heat flux, W
T	temperature, K
x	phase volume fraction, dimensionless

Greek symbols

λ	thermal conductivity, $W m^{-1} K^{-1}$
θ_{eq}	equilibrium contact angle

Subscripts and superscripts

e	effective
G	gas
L	liquid
S	solid

of calculating the effective thermal conductivity as function of the phase volume fractions and thermal conductivities of the components over a range of particle packing density and relative solvent content.

It is possible to derive analytical expressions for the effective thermal conductivity of certain geometrically simple arrangements, notably the limiting cases of conductors in series and in parallel. For conductors in parallel, we have

$$\lambda_e = \sum_{i=G,L,S} x_i \lambda_i \quad (1)$$

where λ_e [$W m^{-1} K^{-1}$] is the effective thermal conductivity, x_i are the volume fractions and λ_i the thermal conductivities of the individual phases. Conductors in parallel represent the theoretical upper bound for λ_e. For conductors in series, which represent the theoretical lower bound, we have

$$\lambda_e^{-1} = \sum_{i=G,L,S} x_i \lambda_i^{-1} \quad (2)$$

Finally, the effective thermal conductivity of ideally mixed phases is their weighted geometric mean

$$\lambda_e = \prod_{i=G,L,S} \lambda_i^{x_i} \quad (3)$$

The dependence of λ_e on x_B for a binary system A–B is shown in Fig. 2 for the above three theoretical cases. For real microstructures, the functional dependence $\lambda_e(\lambda_i, x_i)$

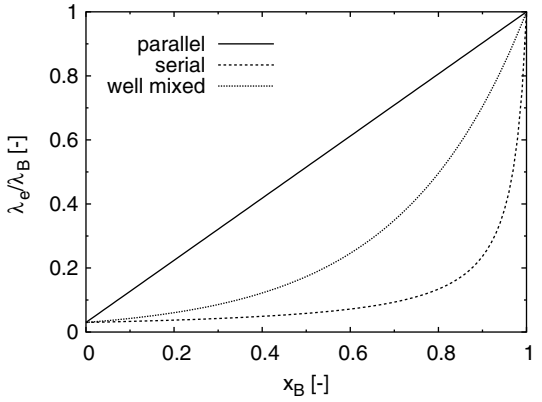

Fig. 2. Effective thermal conductivity of a two-phase system A–B as function of the phase volume fraction of phase B for three theoretical models: conductors in parallel, in series, and well mixed ($\lambda_A = 0.03 W m^{-1} K^{-1}$, $\lambda_B = 1.0 W m^{-1} K^{-1}$).

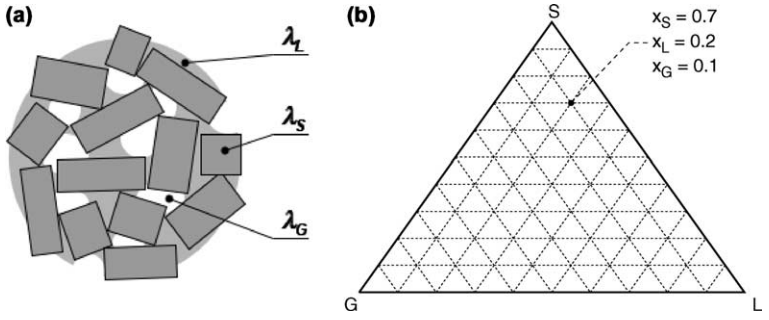

Fig. 1. (a) Schematic three-phase microstructure formed by a packing of rectangular particles and some interstitial liquid. (b) The composition of a three-phase system will be shown on a triangular phase diagram.

has an a priori unknown form, which has to be determined for each class of microstructure individually. One of two approaches is typically used: (i) experimental, by using empirical or semi-empirical expressions, which are usually based on the idea of some mixture of the parallel and serial arrangements or on the Maxwell equation, or (ii) computational, by solving the Fourier's law on a domain that represents the microstructure of interest.

The former approach has been used e.g. for the experimental determination of the effective thermal conductivity of packed beds of porous particles saturated by a binary liquid [4], thermal conductivity of dry sand with varying particle size distribution [5], thermal conductivity of compressed packed beds as function of the compression ratio [6], thermal conductivity of model composite soils [7], thermal conductivity of wet concrete as function of water content [8], thermal conductivity of a packing of seeds as function of moisture content [9], or the conductivity of a packing of multi-sized coarse spheres as function of porosity and water addition [10]. Although many of these cited works deal with multi-phase systems, the reported data ranges are usually too narrow to allow the derivation of generally valid correlations for the calculation of λ_e.

As far as theoretical and computational approaches are concerned, modified versions of the Maxwell's equation for the conductivity of a dispersion of mono-sized spheres in a continuous matrix have been proposed [11–13]. This problem has also been studied computationally by direct numerical simulation [14] and by the combination of a rigorous solution on a two-sphere junction and a network model of the particle packing [15]. Apart from dispersions or packing of spheres, systems with aspherical particles were also studied [16,18], as well as various other structures such as fractals [19,20] or aerogels [21]. Heat conduction in a three-phase system has been considered [22] but a systematic parametric study that would result into the derivation of more generally applicable correlations has not been made to date.

The objective of this work was to develop a method and devise correlations for estimating the thermal conductivity of three-phase microstructures consisting of randomly packed solid particles partially or fully saturated by a liquid phase, valid over a wide range of phase volume fractions and relative conductivities of the components. Note that the problem of finding the effective thermal conductivity of partially liquid-saturated particle packings is similar to that of finding the electrical resistivity index of partially saturated porous media, which has been recently solved by Békri et al. [23]. The main difference is that in the case of thermal conductivity, all three phases are generally conductive, whereas in the mentioned case of electrical resistivity, only one phase was.

2. Methodology

The overall methodology consisted of three steps:

(1) Computational and experimental realisation of three-phase microstructures by systematic variation of the phase volume fractions of the solid and liquid phase, the particle shape and size distribution, the liquid–solid contact angle, and the conductivities of the components.
(2) Computational (by solving the Fourier's law) and experimental (by a transient hot wire method) determination of the effective thermal conductivity for the realised microstructures.
(3) Finding a function $\lambda_e(\lambda_i, x_i)$ that best fits the data sets. This estimator function should be suitable for engineering calculations, we do not require that it be theoretically founded.

2.1. Computational

The computational determination of effective thermal conductivity consists of three steps: (i) microstructure realisation; (ii) solution of the Laplace equation; (iii) calculation of the effective thermal conductivity from converged temperature profile.

Three types of microstructures were used in this work—close random packing of hard and soft spheres, random packing of overlapping cubes, and a random packing of model crystals (rectangular particles with aspect ratio of 4:1). The close packing of particles was generated by the ballistic deposition algorithm [16,17] whereby particles are inserted into the simulation unit cell one at a time. Starting from random position at the top of the cell, they follow a trajectory under the action of two forces: an attractive "gravitational" force which is constant in magnitude and oriented towards the bottom of the unit cell. The other force is a repulsive "collision" force which comes into effect when the incoming particle collides with particles already present in the unit cell. The collision force is proportional to the interparticle overlap by an "elasticity" constant. The particle movement is stopped when the repulsive force exactly offsets the attractive force—usually when the incoming particle rests on three supporting particles having minimised (locally) its potential energy. The elasticity constant determines the final degree of overlap between the particles and it can take values from 0% (hard particles) up to 100% (completely penetrable particles).

The liquid-filled microstructures were generated by adding the required volume fraction of the liquid phase into an existing particle packing in the form of discrete droplets that were placed into random positions and subsequently allowed to spread to its equilibrium position by the Volume-of-Fluid algorithm [24]. The local equilibrium position of a liquid cluster is defined as

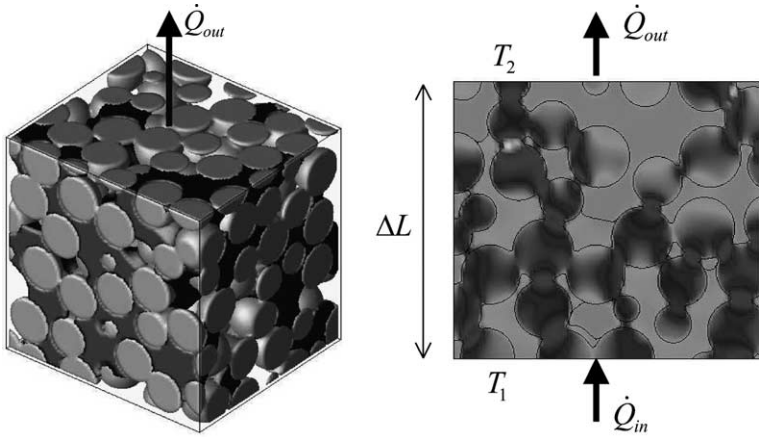

Fig. 3. Unit cell for calculating the effective thermal conductivity. A temperature gradient is applied across the unit cell and the Fourier's law is solved until convergence, λ_e is then calculated from the steady-state heat flux. The cross-section shows the field of norms of the heat flux at steady state, gray-scale levels are proportional to the heat flux intensity.

such spatial arrangement in which the liquid–gas interfaces have a constant curvature and the equilibrium contact angle is satisfied at all three-phase contact lines [25].

The next step was the solution of the Fourier's law on a cubic unit cell of size L containing the microstructure of interest (see Fig. 3). At steady state, the accumulation terms are zero and the differential enthalpy balance has the form

$$\nabla(\lambda \nabla T) = 0 \tag{4}$$

where T [K] is temperature and $\lambda = \lambda(\mathbf{x})$ is the local thermal conductivity, as defined by the microstructure (i.e., λ_S, λ_L, λ_G). The boundary conditions are $T = T_1$ at $z = 0$, $T = T_2$ at $z = L$, and $\nabla T = 0$ at $x = 0$, $x = L$, $y = 0$, and $y = L$ (i.e., a macroscopic temperature gradient $(T_2 - T_1)/L$ is imposed across the unit cell in the z-direction and insulating walls are imposed in the x- and y-directions). The Laplace equation (Eq. (4)) was solved numerically on a grid of $100 \times 100 \times 100$ points using finite difference discretisation and the successive over-relaxation method [26].

The effective thermal conductivity was then calculated from the converged temperature field from the formula

$$\lambda_e = -\frac{\dot{Q}_1}{A}\frac{L}{(T_2 - T_1)} \tag{5}$$

where L is the size of the unit cell in the z-direction, A is the cross-section area of the unit cell perpendicular to the z-direction (in our case $A = L^2$), $(T_2 - T_1)$ is the temperature difference across the unit cell and $\dot{Q}_1$ is the overall heat flux into the unit cell, obtained by integrating the fluxes across the inlet face of the unit cell

$$\dot{Q}_1 = \int_A -\lambda \frac{\partial T}{\partial z}\,\mathrm{d}x\,\mathrm{d}y \tag{6}$$

($\dot{Q}_2$ could be used as well because at steady state there is no net accumulation of heat in the unit cell and so $\dot{Q}_1$ and $\dot{Q}_2$ are equal.)

2.2. Experimental

A commercially available instrument KD2 (Decagon Devices Inc., USA), which is based on the transient hot wire method [27], was used for the measurement of effective thermal conductivity in this work. A thermal grease was applied to the hot wire probe when measuring dry samples in order to ensure good thermal contact between the probe and the particles. Glass beads (Sovitec, Belgium) of various sizes were used as model particles for the experiments. In particular, four size classes of glass beads were used, named "AH", "AF", "AC", and "BL", with mean diameters $d_{50} = 68$, $d_{50} = 112$, $d_{50} = 200$, and $d_{50} = 628\,\mu$m, respectively. Deionised water was used as model liquid. All measurements were performed at ambient conditions (~25 °C, normal pressure).

3. Results and discussion

3.1. Effect of phase volume fractions

The effect of the volume fractions x_i of the gas, liquid, and solid phases on the effective thermal conductivity λ_e of a particle packing partially saturated by a liquid was investigated first. Since the random close packing of uniform spheres would only give one value of packing density, several random packings were generated by the

ballistic deposition algorithm from spheres of two sizes ($d_1 = 4d_2$) by systematically varying the ratio at which the smaller and the larger spheres were mixed (n_1:n_2 = 1:1, 1:2, 1:4, and 1:8). By further changing the particle "elasticity" parameter in the deposition algorithm, packing densities in the range $0.50 < x_S < 0.70$ were eventually generated.

For each value of x_S, the relative volume fraction of the liquid phase, $x'_L \equiv x_L/(1 - x_S)$, was varied from 0.0 to 1.0 by random addition of liquid droplets with diameter d_2 into the particle packing and then letting each liquid-phase cluster spread into its equilibrium position. Both hydrophilic ($\theta_{eq} = 0°$) and hydrophobic ($\theta_{eq} = 90°$) conditions were generated. An example of one microstructure is shown in Fig. 4b.

The effective thermal conductivity was then calculated for each realisation of the microstructure by solving the Fourier's law as described in Section 2. The component conductivities were set to typical values of $\lambda_S = 1.0$, $\lambda_L = 0.1$, and $\lambda_G = 0.01\,W\,m^{-1}\,K^{-1}$. The complete set of simulation results is shown in Fig. 5. The effective thermal conductivity is plotted in a dimensionless form (scaled by λ_S). This allows the recalculation of the dimensional thermal conductivity λ_e also for other systems by simple multiplication by λ_S, as long as the ratio λ_S/λ_L remains constant. Rescaling for general λ_S/λ_L ratios is discussed in Section 3.3.

The results suggest that the dependence $\lambda_e(x_L)$ for constant x_S could be approximated by a linear function in this region of the phase space, which means that when conductivities for the end points (i.e., $x'_L = 0.0$ and $x'_L = 1.0$) are know from experiments, simulation, or from an estimation function, the rest can be calculated by linear interpolation. Experimentally measured dependence $\lambda_e(x_L)$ for mono-dispersed glass beads ($d_{50} = 200\,\mu m$) wetted by water is shown in Fig. 6 and compared with simulations for the same system. The simulations are in a relatively good agreement with experiments for higher values of liquid saturation, while for dry systems the effective thermal conductivity is overpredicted by the simulations. This is most probably due to poor approximation of singular contacts between

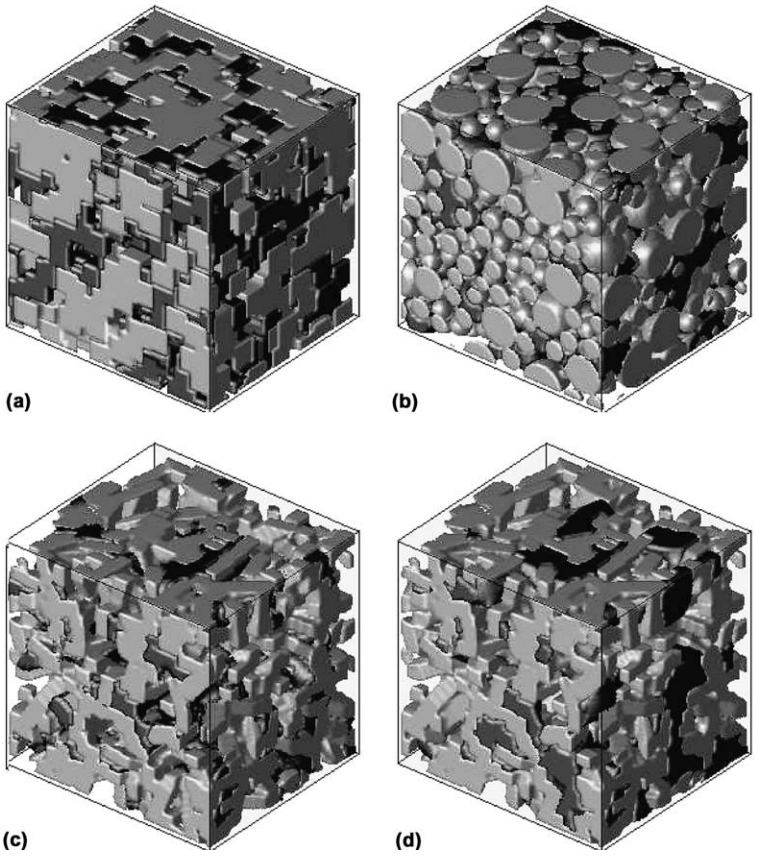

Fig. 4. Examples of microstructures used for the calculation of effective thermal conductivity: (a) random filling of overlapping cubes; (b) close random packing of a binary mixture of hard spheres partially filled by a wetting liquid; (c) and (d) random assembly of rectangular particles with aspect ratio 4:1, partially filled by a wetting and non-wetting liquid, respectively.

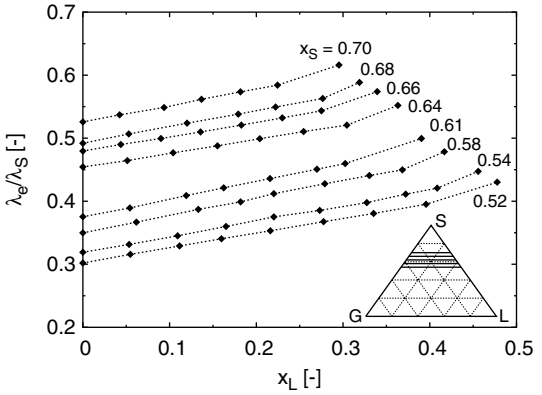

Fig. 5. Computer simulation results of the dependence of effective thermal conductivity on composition for close random packing of spheres in the range of $0.50 < x_S < 0.70$ and a full range of $0.0 < x'_L < 1.0$ for each x_S (the dotted lines connect points of constant x_S, the values are indicated). The individual conductivities are $\lambda_G = 0.01$, $\lambda_L = 0.1$, and $\lambda_S = 1.0\,W\,m^{-1}\,K^{-1}$; the spheres are hydrophilic, $\theta_{eq} = 0°$. The insert shows the region covered by this simulation in the phase diagram.

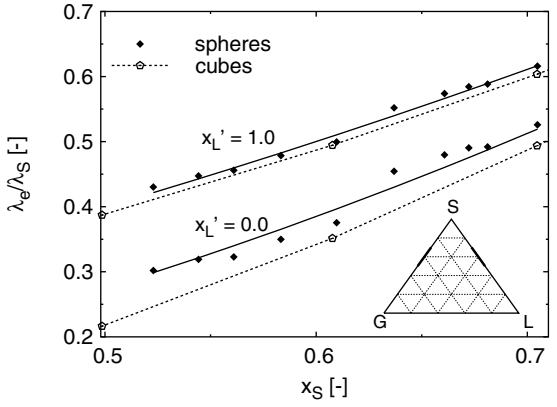

Fig. 7. Computer simulation results of the dependence of effective conductivity on the phase volume fraction of the solid phase for completely dry ($x'_L = 0.0$) and wet ($x'_L = 1.0$) close random packing of spheres and a random filling of cubes ($\lambda_G = 0.01$, $\lambda_L = 0.1$, and $\lambda_S = 1.0\,W\,m^{-1}\,K^{-1}$). The full lines are power-law fits for spheres, dotted lines are trendlines for cubes. The insert shows the region covered by this simulation in the phase diagram.

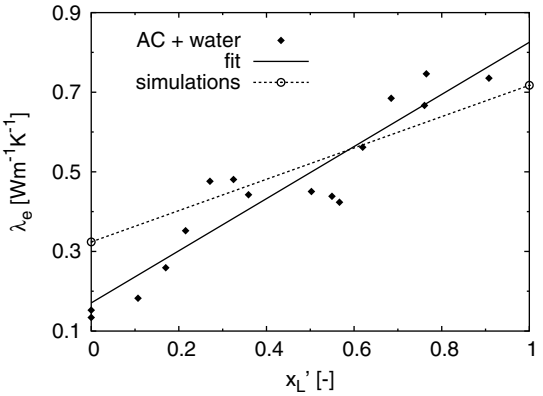

Fig. 6. Dependence of effective thermal conductivity on the relative volume fraction of the liquid phase for a close random packing of glass spheres type "AC" ($d_{50} = 200\,\mu m$) with water as the liquid phase obtained experimentally and by numerical simulations. The thermal conductivities are $\lambda_{H_2O} = 0.61\,W\,m^{-1}\,K^{-1}$ for water and $\lambda_{air} = 0.02\,W\,m^{-1}\,K^{-1}$ for air, the dry packing density is $x_S = 0.61$ and the thermal conductivity of this glass is $\lambda_{glass} = 0.8\,W\,m^{-1}\,K^{-1}$.

the beads by the finite difference discretisation scheme which has been used.

As mentioned above, if the effective conductivity of the two binary systems (dry and fully saturated particle packing) is known, then the effective conductivity of the intermediate cases ($0.0 < x'_L < 1.0$) can be obtained by interpolation. The dependence $\lambda_e(x_S)$ for $x'_L = 0.0$ and $x'_L = 1.0$ obtained from computer simulations is shown in Fig. 7. Within this range of x_S even this dependence could be approximated by a linear function but it will be shown below that a power-law function can be found that fits the data over a wider range of solid phase volume fractions (this power-law fit is already shown in Fig. 7 as the solid lines).

The dependence of λ_e on x_S for a dry system was also measured experimentally. Different values of x_S were realised by mixing glass beads of two different sizes in various ratios. The coarse fraction were beads of type BL and the two fine fractions were beads of type AF and AH. Four data sets are shown in Fig. 8, correspond-

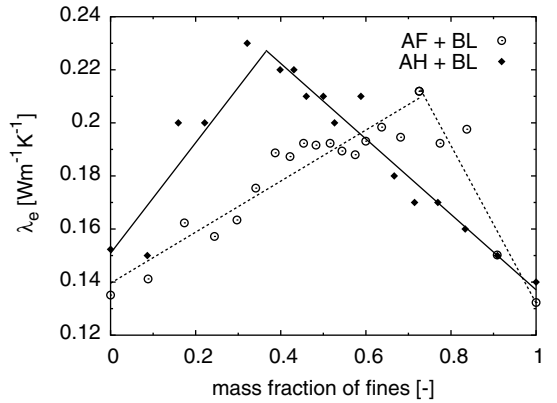

Fig. 8. Experimentally measured dependence of effective thermal conductivity on composition for binary mixtures of coarse and fine glass spheres. The sphere diameters are $d_{50} = 638\,\mu m$ for type "BL", $d_{50} = 112\,\mu m$ for type "AF", and $d_{50} = 68\,\mu m$ for type "AH".

ing to mixtures AF–BL and AH–BL where in each case the fine particles were gradually added to the coarse ones and vice versa. The maximum packing density and thus the maximum effective thermal conductivity was higher for the AH–BL mixture than for AF–BL because the AH particles fit better into the void space of a packing of BL particles thanks to their smaller size. The actual dependence of the packing density x_S on the mixing ratio for the AH–BL system is shown in Fig. 9 together with a schematic illustration of the packing of a binary mixture. The maximum corresponds to a situation when additional fine particles no longer fit into the void space between the coarse ones and instead start to act as spacers that dilute the original close-packed structure of the coarse particles. This situation occurs for a higher mass fraction of added fine particles in the case of the AF-BL system. The combination of the dependence of λ_e on the mixing ratio with the dependence of x_S on the mixing ratio allows the comparison of experimentally measured data with prediction by numerical simulations, such as those in Fig. 7.

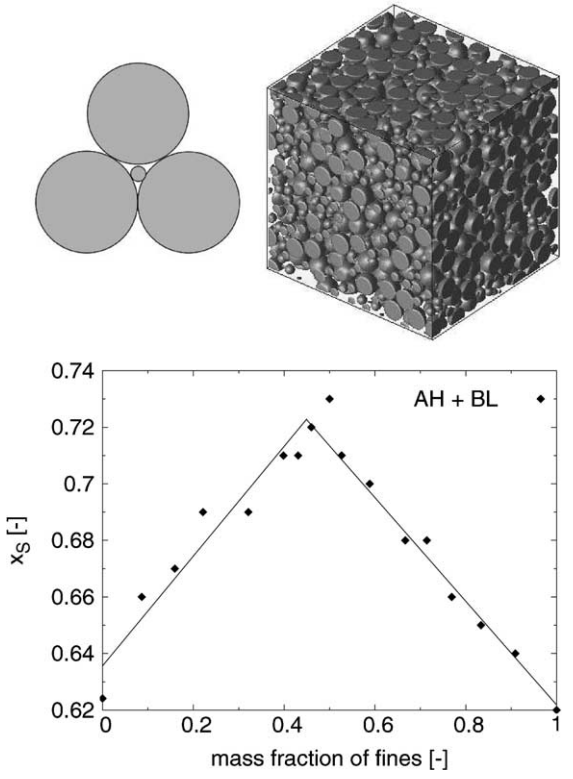

Fig. 9. Illustration of a situation where a fine particle fits into the void space created by a packing of the coarse particles and an example of a packing of a mixture of coarse and fine spheres where the fine particles act as "spacers" that dilute the coarse particle packing (top). Dependence of the packing density on mixing ratio (bottom).

3.2. Effect of microstructure

The effect of the spatial arrangement of the phases on effective conductivity was investigated next. Microstructure can be affected by the particle shape in the case of the solid phase, or particle wettability in the case of the liquid phase. The computer simulation study presented in Fig. 5 was performed for both hydrophilic and hydrophobic particles and the results were, somewhat against expectation, practically identical. Microstructures representing a random packing of model crystals (rectangular particles with aspect ratio 4:1) were also generated and filled with both wetting and non-wetting liquid phase in the entire range $0.0 < x'_L < 1.0$. These microstructures are shown in Fig. 4c and d.

The dependence $\lambda_e(x_L)$ for hydrophobic and hydrophilic crystals is compared with that of a packing of hydrophilic spheres with the same phase volume fraction of the solid phase ($x_S = 0.64$) in Fig. 10. As can be seen, in this range of parameters there is practically no difference between the microstructures. To find out if there is an effect for other values of x_S in the range $0.5 < x_S < 0.7$, which is of interest for drying, the effective conductivity for the limiting dry ($x'_L = 0.0$) and wet ($x'_L = 1.0$) cases for a random packing of hard spheres was compared with that of a random assembly of overlapping cubes (microstructure in Fig. 4a). This comparison is shown in Fig. 7 and it is evident that while there is little difference for the wet case, the two systems start to deviate somewhat more for lower values of x_S in the dry case. Since identical microstructures of the solid phase were used for each x_S and the only difference was the conductivity of the fluid phase ($\lambda_L = 0.1$ and

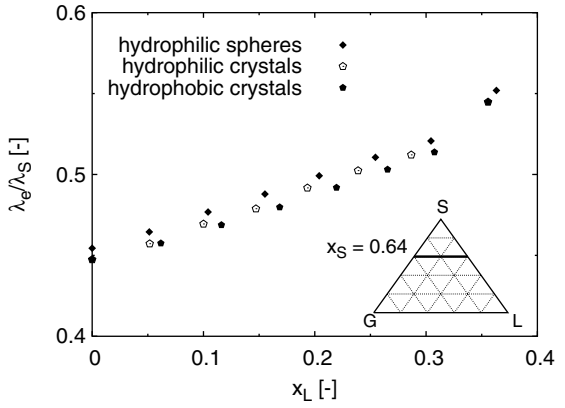

Fig. 10. Comparison of computed effective thermal conductivity of hydrophilic spheres with that of hydrophilic and hydrophobic rectangular particles (crystals) as function of x_L (the microstructures are shown in Fig. 4). The individual conductivities are $\lambda_G = 0.01$, $\lambda_L = 0.1$, and $\lambda_S = 1.0\,W\,m^{-1}\,K^{-1}$; $x_S = 0.64$ for all three systems, as shown in the inserted triangular phase diagram.

$\lambda_G = 0.01\,W\,m^{-1}\,K^{-1}$), this deviation is due to the component conductivities (their ratio).

3.3. Effect of component conductivities

To investigate further the effect that component conductivities have on the overall conductivity of a given microstructure, a series of simulations for a binary system A–B was performed, whereby the ratio of the component conductivities λ_B/λ_A was systematically varied in the range of 2:1, 5:1, 10:1, 20:1, 50:1, and 100:1. Two different absolute values of λ_A were used, $\lambda_A = 0.1$ and $\lambda_A = 0.01\,W\,m^{-1}\,K^{-1}$, and some of the ratios (e.g., 10:1) were realised for both of these values. The microstructures were random assemblies of overlapping cubes of phase B in (initially continuous) phase A. The microstructures can thus be interpreted as completely "dry" or "wet" versions of the microstructure shown in Fig. 4a.

The results of the computational study are shown in Fig. 11. All data sets were fitted by a power-law function (in fact Archie's law) of the form

$$\lambda_e = (\lambda_B - \lambda_A)x_B^c + \lambda_A \tag{7}$$

where the exponent c depends on the ratio of conductivities λ_B/λ_A and this dependence is generally different for each class of microstructure. Eq. (7) gave the best fit of the data (in terms of the mean square error) compared with other functions that were tried, e.g. various weighted averages of the parallel, serial, and well-mixed cases where the weights were the fitting parameters. The dependence of the exponent c on the ratio of conductivities λ_B/λ_A is shown in Fig. 12 for two microstructures—the random close packing of hard spheres (Fig. 4b) and the random assembly of overlapping cubes (Fig. 4a).

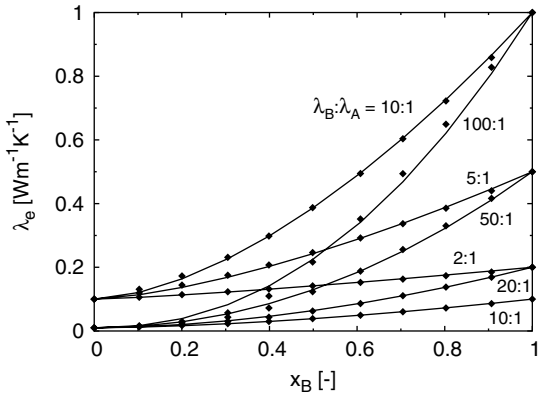

Fig. 11. Computer simulation results of the dependence of effective thermal conductivity of a binary system A–B (random assembly of cubes) on the volume fraction of component B for several ratios of the component thermal conductivities λ_B/λ_A as indicated by the curves. The solid lines are fits by a power-law estimator function.

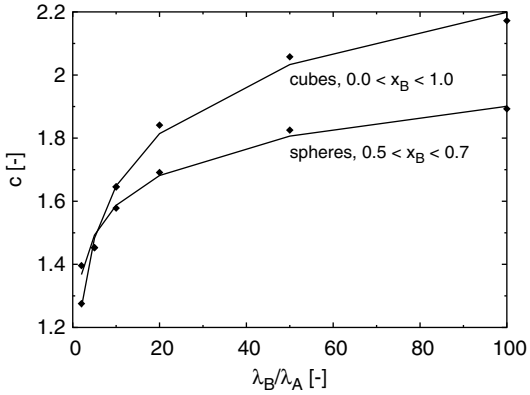

Fig. 12. Dependence of the exponent c from the power-law estimator function on the ratio of component thermal conductivities λ_B/λ_A for random assembly of cubes and a random close packing of spheres. The validity regions in terms of x_B are indicated by the curves.

The curves were fitted by logarithmic functions; for spheres,

$$c = 0.136\log(\lambda_B/\lambda_A) + 1.27 \tag{8}$$

and for cubes,

$$c = 0.239\log(\lambda_B/\lambda_A) + 1.10 \tag{9}$$

These correlations are valid in the range $2 < \lambda_B/\lambda_A < 100$ and x_B as indicated in Fig. 12. As has been mentioned in the discussion following Fig. 7, the difference between the two microstructures is more profound for higher values of the ratio λ_B/λ_A. The functional dependence $c(\lambda_B/\lambda_A)$ can be generated for other classes of microstructures that would be of interest, using the same computational methodology.

3.4. General three-phase systems

Eq. (7) allows the estimation of the effective thermal conductivity of binary systems. For ternary and generally n-ary systems, it can be applied hierarchically by defining a sequence of binary pseudocomponents and interpolating between them. For example, in the case of a ternary gas–liquid–solid (G–L–S) system, one would first estimate the conductivity of the binary systems G–S and L–S using the actual volume fraction of the solid phase x_S. Then the appropriate value of the exponent c would be found, i.e. $c(\lambda_S/\lambda_L)$ for L–S and $c(\lambda_S/\lambda_G)$ for G–S. Finally, one would interpolate between the "dry" (G–S) and "wet" (L–S) pseudocomponents using the relative volume fraction of the liquid phase $x'_L \equiv x_L/(1 - x_S)$.

This is demonstrated in Fig. 13, where the data points are the results of computer simulations on cubic microstructure (Fig. 4) over the entire range of phase volume fractions, i.e. $0.0 < x_S < 1.0$ and $0.0 < x'_L < 1.0$. The

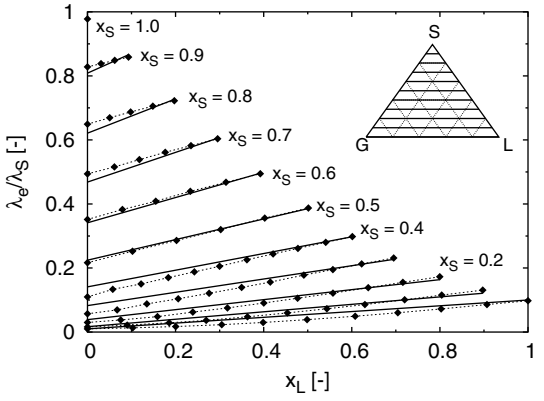

Fig. 13. Computer simulation results of the dependence of effective thermal conductivity of random assembly of uniform cubes (microstructure is shown in Fig. 4a) on composition, covering the entire range of phase volume fractions as shown in the inserted phase diagram. The full lines show estimates obtained by linear interpolation between conductivities of binary pseudocomponents calculated from a power-law function, the dashed lines join points of constant x_S to guide the eye ($\lambda_G = 0.01$, $\lambda_L = 0.1$, and $\lambda_S = 1.0\,W\,m^{-1}\,K^{-1}$).

solid lines are linear interpolations between binary pseudocomponents (G–S and L–S) whose conductivities were estimated using Eq. (7). The conductivity estimated for the L–S pseudocomponent is nearly perfect; for the G–S pseudocomponent there are small errors due to the relatively large ratio λ_S/λ_G, but taken over the entire phase plane the prediction is satisfactory for the purpose of engineering calculations.

4. Conclusions

The effect of composition and microstructure on the effective thermal conductivity of particle assemblies partially wetted by a liquid, was investigated. The effective thermal conductivity was mapped over a broad range of phase volume fractions and ratios of individual component conductivities, and the data were fitted by a relatively simple power-law correlation suitable for a priori estimation of effective thermal conductivity for chemical engineering calculations. The methodology presented in this work is general and can be used for the estimation of effective thermal conductivity of various two-, three-, and multi-phase systems such as suspensions, emulsions, foams or composite materials, e.g. polymer blends, pastes, or even biological tissues.

Acknowledgments

Research funding from GlaxoSmithKline is gratefully acknowledged. The glass bead samples were kindly provided by F. Juprelle from Sovitec.

References

[1] R.B. Keey, Drying of Loose and Particulate Materials, Hemisphere Publishing Corporation, New York, 1993, pp. 163–175.
[2] C.L. Lin, J.D. Miller, Pore structure and network analysis of filter cake, Chem. Eng. J. 80 (2000) 221–231.
[3] R.Y. Yang, R.P. Zhou, A.B. Yu, Numerical study of the packing of wet coarse uniform spheres, AIChE J. 49 (2003) 1656–1666.
[4] W. Blumberg, E.U. Schlunder, Thermal conductivity of packed beds consisting of porous particles wetted with binary mixtures, Chem. Eng. Proc. 34 (1995) 339–346.
[5] I.H. Tavman, Effective thermal conductivity of granular porous materials, Int. Commun. Heat Mass Transfer 23 (1996) 169–176.
[6] G. Widenfeld, Y. Weiss, H. Kalman, The effect of compression and preconsolidation on the effective thermal conductivity of particulate beds, Powder Technol. 133 (2003) 15–22.
[7] N.H. Abu-Hamdeh, R.C. Reeder, Soil thermal conductivity: effects of density, moisture, salt concentration, and organic matter, Soil Sci. Soc. Am. J. 64 (2000) 1285–1290.
[8] N. Mendes, C.P. Fernandes, P.C. Philippi, R. Lamberts, Moisture content influence on thermal conductivity of porous building materials, in: Proc. 7th Int. IBPSA Conf., Rio de Janeiro, Brazil, August 2001, pp. 957–964.
[9] W. Yang, S. Sokhansanj, J. Tang, P. Winter, Determination of thermal conductivity, specific heat and thermal diffusivity of borage seeds, Biosys. Eng. 82 (2002) 169–176.
[10] R.P. Zou, J.Q. Xu, C.L. Feng, A.B. Yu, S. Johnson, N. Standish, Packing of multi-sized mixtures of wet coarse spheres, Powder Technol. 130 (2003) 77–83.
[11] Y.C. Chiew, E.D. Glandt, The effect of structure on the conductivity of a dispersion, J. Coll. Interf. Sci. 94 (1983) 90–104.
[12] V.R. Raghavan, H. Martin, Modeling of 2-phase thermal conductivity, Chem. Eng. Proc. 34 (1995) 439–446.
[13] E.E. Gonzo, Estimating correlations for the effective thermal conductivity of granular materials, Chem. Eng. J. 90 (2002) 299–302.
[14] I.C. Kim, S. Torquato, Effective conductivity of suspensions of overlapping spheres, J. Appl. Phys. 71 (1992) 2727–2735.
[15] C. Argento, D. Bouvard, Modeling the effective thermal conductivity of random packing of spheres through densification, Int. J. Heat Mass Transfer 39 (1996) 1343–1350.
[16] D. Coelho, J.-F. Thovert, P.M. Adler, Geometrical and transport properties of random packings of spheres and aspherical particles, Phys. Rev. E 55 (1997) 1959–1977.
[17] F. Stepanek, P.B. Warren, Computer-aided design of granule microstructure, Paper G4.1, CHISA 2002, Prague, Czech Republic, August 25–29, 2002.
[18] M. Gupta, J. Yang, C. Roy, Modelling of effective thermal conductivity in polydispersed bed systems: a unified approach using the linear packing theory and unit cell model, Can. J. Chem. Eng. 80 (2002) 830–839.

[19] J.-F. Thovert, F. Wary, P.M. Adler, Thermal conductivity of random media and regular fractal, J. Appl. Phys. 68 (1990) 3872–3883.
[20] Y. Xuan, Q. Li, W. Hu, Aggregation structure and thermal conductivity of nanofluids, AIChE J. 49 (2003) 1038–1043.
[21] A.P. Roberts, Morphology and thermal conductivity of organic aerogels, Phys. Rev. E 55 (1997) 1286–1289.
[22] D.P. Bentz, E.J. Garboczi, D.A. Quenard, Modelling drying shrinkage in reconstructed porous materials: application to porous Vycor glass, Mod. Simul. Mater. Sci. Eng. 6 (1998) 211–236.
[23] S. Békri, J. Howard, J. Muller, P.M. Adler, Electrical resistivity index in multiphase flow through porous media, Transp. Porous Media 51 (2003) 41–65.
[24] R. Scardovelli, S. Zaleski, Direct numerical simulation of free-surface and interfacial flow, Annu. Rev. Fluid Mech. 31 (1999) 567–603.
[25] F. Stepanek, M. Marek, P.M. Adler, The effect of pore space morphology on the performance of anaerobic granular sludge particles containing entrapped gas, Chem. Eng. Sci. 56 (2001) 467–474.
[26] W.H. Press, B.P. Flannery, S.A. Teukolsky, W.T. Vetterling, Numerical Recipes in Fortran, Cambridge University Press, Cambridge, UK, 1992, pp. 857–861.
[27] A.J. Fontana, B. Wacker, C.S. Campbell, G.S. Campbell, Simultaneous thermal conductivity, thermal resistivity, and thermal diffusivity measurement of selected foods and soils, Paper 01-6101, ASAE Annual Meeting, Sacramento, CA, July 29–August 1, 2001.